

Observation of many-body coherence in quasi-one-dimensional attractive Bose gases

Hikaru Tamura,^{1,*} Sambit Banerjee,¹ Rongjie Li,¹ Panayotis Kevrekidis,^{2,3} Simeon I. Mistakidis,⁴ and Chen-Lung Hung^{1,5,†}

¹*Department of Physics and Astronomy, Purdue University, West Lafayette, IN 47907, USA*

²*Department of Mathematics and Statistics, University of Massachusetts Amherst, Amherst, Massachusetts 01003-9305, USA*

³*Department of Physics, University of Massachusetts Amherst, Amherst, Massachusetts 01003, USA*

⁴*Department of Physics and LAMOR, Missouri University of Science and Technology, Rolla, MO 65409, USA*

⁵*Purdue Quantum Science and Engineering Institute, Purdue University, West Lafayette, IN 47907, USA*

(Dated: June 17, 2025)

Macroscopic coherence is an important feature of quantum many-body systems exhibiting collective behaviors, with examples ranging from atomic Bose-Einstein condensates, and quantum liquids to superconductors. Probing many-body coherence in a dynamically unstable regime, however, presents an intriguing and outstanding challenge in out-of-equilibrium quantum many-body physics. Here, we experimentally study the first- and second-order coherence of degenerate quasi-one-dimensional (1D) Bose gases quenched from repulsive to modulationally unstable attractive interaction regimes. The resulting dynamics, monitored by in-situ density and matter-wave interference imaging, reveals phase-coherent density wave evolutions arising from the interplay between noise-amplified density modulations and dispersive shock waves of broad interest within nonlinear physics. At longer times, the gases become phase-scrambled, exhibiting a finite correlation length. Interestingly, following an interaction quench back to the repulsive regime, we observe that quasi-long-range coherence can be spontaneously re-established. This captivating rephasing dynamics can be attributed to the nucleation and annihilation of density defects in the quasi-1D geometry. These results shed light on out-of-equilibrium phase coherence in quantum many-body systems in a regime where beyond mean-field effects may arise and theoretical approaches have not been well-established.

Long-range phase coherence is a defining feature of Bose-Einstein condensates (BECs) [1] and superfluidity [2]. It plays a critical role not only in equilibrium but also in out-of-equilibrium conditions dictating quantum superposition and interference since it quantifies crosstalk of atoms at long distances. A global quench in ultracold gases offers an ideal setting for studying nonequilibrium quantum dynamics, assessing observations of prethermalization [3] and recurrent dynamics [4] in 1D Bose gases, phase scrambling and rephasing in dipolar gases [5], as well as dynamical scaling of correlation functions through a quantum [6–8] or classical phase transition [9].

Attractive gases and their phase coherence, unlike their stable repulsive counterparts, are known to suffer modulational instability (MI). This mechanism triggers the amplification of small fluctuations and leads to the formation of localized solitonic structures [10–13]. In $D > 1$ dimensions, growing waves in MI introduce wave collapse [14–17] at a dominant unstable length scale determined by the interaction strength, i.e., the healing length. The wave collapse is responsible for spontaneously forming bright solitons and arrays thereof [12, 17, 18]. Bright solitons have by now been showcased to be ubiquitously possible to produce across harmonically trapped atomic gases. These include ${}^7\text{Li}$ [19], where solitonic pairs were realized, ${}^{85}\text{Rb}$ [20], for examining soliton-barrier interac-

tions, and a solitonic atom interferometer [21], as well as ${}^{39}\text{K}$ [22].

Beyond spatially separated solitons, attractive gases in 1D could exhibit very rich out-of-equilibrium behavior during the nonlinear stage of MI [23–25]. It is known that 1D Schrödinger models with self-focusing cubic-nonlinearity feature infinitely many conservation laws. Indeed, the associated integrability enables the identification of numerous families of special solutions, including those of spatially or temporally periodic breather solutions [26, 27], whose formation process [28, 29] has recently attracted great attention [30, 31]. Their evolution represents dynamical energy exchange between unstable modes within a modulationally unstable background. This manifests itself in the phase sector as transitions between complete π phase jumps and a homogeneous phase profile. As a direct consequence of integrability in 1D, the conservation laws prevent breathers from decaying into phase uncorrelated solitons [32]. Phase coherence thus provides a decisive factor to rule out the existence of phase-uncorrelated excitations. However, out-of-equilibrium phase coherence beyond solitary waves in attractive many-body systems, especially in quantum gas experiments, remains largely unexplored.

Here, we report observation of dynamical evolution of many-body coherence in quasi-1D Bose gases quenched from repulsive to attractive interactions. Our quasi-1D gases differ significantly from harmonically trapped ones. As illustrated in Fig. 1a, the gas is confined by an elongated optical box trap, featuring prethermalized density fluctuations over a homogeneous background (see [33])

* tamurah@ims.ac.jp; Present address: Institute for Molecular Science, Okazaki, Aichi 444-8585, Japan

† clhung@purdue.edu

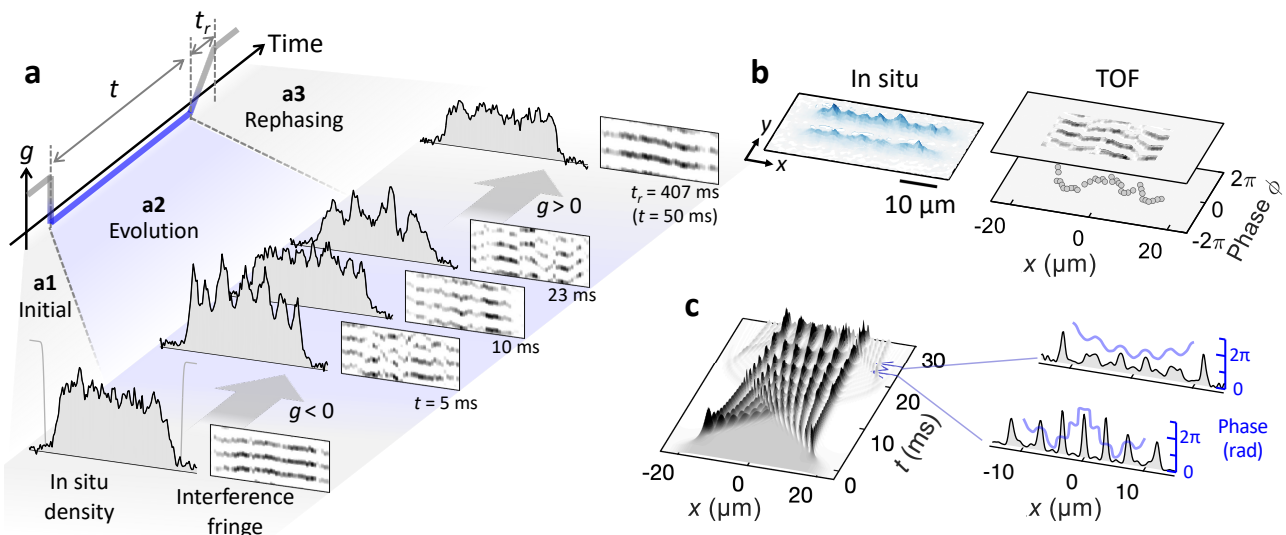


Fig. 1. **Dynamical density modulations and phase coherence of quasi-1D attractive Bose gases in a box.** **a**, A repulsively interacting atomic superfluid (a1) is quenched to the weakly attractive regime where it is held for time t (a2). The interaction is then slowly brought back to its initial repulsive value, triggering dynamical rephasing (a3). **b**, In each experimental realization, two quasi-1D gases are prepared in parallel. They are imaged in situ or released to produce matter-wave interference via an in-plane time-of-flight (TOF) before imaging. A local relative phase ϕ is obtained from the extracted interference fringes. Prototypical in-situ densities and interference patterns right before the quench (a1), for different hold times (a2), and after a long ramp (a3) are displayed in **a**. **c**, 1D GPE simulation of an ideal wavefunction confined in a Gaussian wall box and quenched from repulsive to attractive interactions. The black (blue) solid lines represent density (phase) profiles at the times indicated by the arrows.

and sharp density gradients at the edges in the initial superfluid phase (a1). After an interaction quench (a2), the gas evolves towards displaying not only noise-amplified density modulations in the bulk but also shock waves arising from the edges. By monitoring local density and phase fluctuations through in-situ imaging and matter-wave interference, respectively, we observe the resulting dynamical generation of density modulations with preserved phase coherence. Interestingly, this emerging signature represents neither solitons nor breathers but non-insulated density and phase profiles as remnants of the nonlinear stage of MI in quasi-1D, as visualized by the first- and second-order coherence. At longer hold times, we find that the phase correlation length scale is shortened to the healing length, which we attribute to global dephasing.

Exploiting a reverse quench, that is, ramping the interaction from attractive back to its initial repulsive value, the system returns to a modulationally stable regime (a3). We observe that quasi-long-range phase coherence re-establishes progressively at slower ramps. Both our experiments and mean-field simulations indicate that density modulations at the attractive interaction convert to dark solitary waves in the repulsive interaction regime. Our studies on defect dynamics suggest the importance of extended dimensionality beyond pure 1D phenomenology, where we attest that mechanisms for defect annihilation [34–36] are responsible for reinstating the global phase coherence.

Our experiment begins with loading a nearly pure cesium BEC into two parallel quasi-1D boxes; see [33] for details. Each box has length $l = 40 \mu\text{m}$ along the longitudinal (x -)axis. The transverse trap frequencies are $(\omega_y, \omega_z) \approx 2\pi \times (68, 2.2 \times 10^3) \text{ Hz}$, giving harmonic oscillator lengths $(l_y, l_z) \approx (1.1, 0.18) \mu\text{m}$ and high trap aspect ratios $(\frac{l}{l_y}, \frac{l}{l_z}) \approx (36, 220)$. After an initial trap loading at a s -wave scattering length of $105a_0$, where a_0 is the Bohr radius, we quench to a weakly negative value $a \approx -5a_0$ by controlling a magnetic Feshbach resonance [37]. The initial interaction energy $n|g| \approx \hbar \times 76 \text{ Hz}$ is comparable to the trap vibrational energy $\hbar\omega_y$, leading to a transverse motion that damps out in the first 3 ms followed by a gradual atom loss [33]. Here, $g \approx 2\hbar^2 a / (ml_y l_z)$ the 1D interaction parameter, $n \approx 400 \mu\text{m}^{-3}$ the effective 1D density, $\hbar = 2\pi\hbar$ the Planck constant, and m the atomic mass. Because of a tighter confinement, the atomic motion along the z -axis remains approximately in the ground state throughout the quench dynamics.

The density profiles of the quenched gases are monitored by in situ density imaging (left panel in Fig. 1b). To probe phase coherence, we adapt a matter-wave-interference technique [38, 39]. After a hold time t , we perform time-of-flight (TOF) imaging in the x - y plane. The parallel gases expand quickly along the y -axis due to large aspect ratio and interfere, yielding information about their relative phase $\phi(x)$ longitudinally; see Fig. 1b.

Quench dynamics of a 1D homogeneous quantum gas

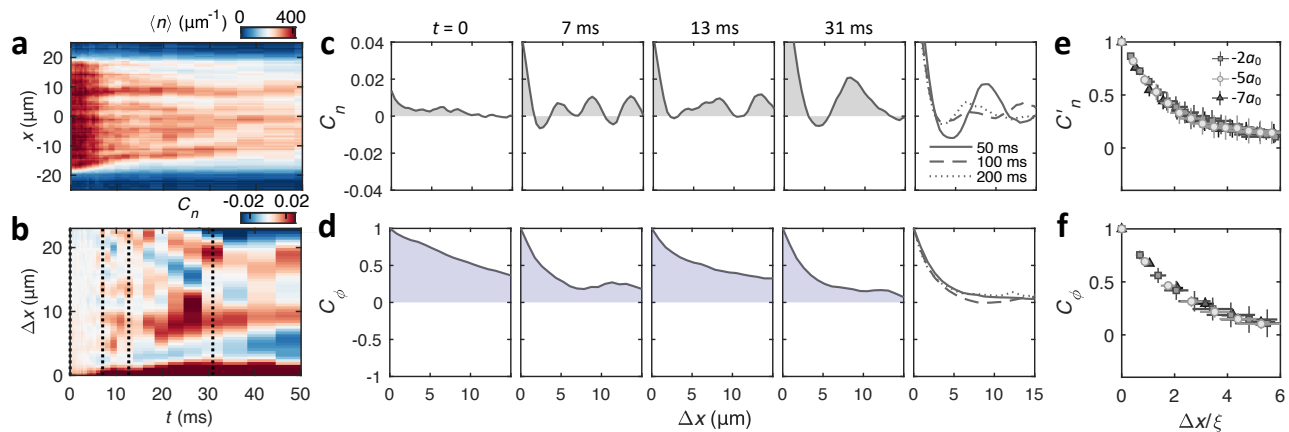


Fig. 2. **Observation of dynamical density modulations and phase coherence of quenched quasi-1D Bose gases.** **a**, Time evolution of the sample-averaged density profile after a quench of s-wave scattering length from $a \approx 105a_0$ to $-5a_0$. The density is integrated over the transverse directions and plotted along the x -axis. **b**, Dynamics of density-density correlation function $C_n(\Delta x)$ with two-point separation Δx . **c**, $C_n(\Delta x)$ at the characteristic times marked by dashed lines in **b**, and at the indicated long hold times. **d**, Two-point phase correlation function $C_\phi(\Delta x)$ at the same times. **e**, Normalized density-density correlation function $C'_n = C_n(\Delta x)/C_n(0)$ and **f**, C'_ϕ versus rescaled length $\Delta x/\xi$ at three different post-quench scattering lengths. C'_n and C'_ϕ are time-averaged over samples measured after hold time $t = 50$ ms. The vertical error bars show the standard deviation from the time-averaged values. The horizontal error bars stem from the uncertainty in the determination of the scattering length.

with sharp edges can be mapped to a recently studied dam-break problem [29, 40]. Upon an interaction quench the initial sharp density gradients at the edges produce a pair of dispersive shock waves (DSWs) [41] that evolve through the nonlinear stage of MI [24]. The DSW is a rapidly oscillating wave structure that is self-similarly modulated at a slower scale and is sustained by the competition of wave steepening and dispersion. More broadly, this setting is closely related to the so-called Riemann problems involving initial density or velocity jumps that have recently attracted extensive interest in dispersive nonlinear systems [42].

To understand density and phase evolutions purely originating from DSWs, we first deploy numerical simulations of the 1D mean-field Gross-Pitaevskii equation (GPE). We start with the ground state of the gas confined in a box with Gaussian-wall width $3 \mu\text{m}$ approximating the experimental potential, and the scattering length is quenched from $105a_0$ to $-4.6a_0$. The produced DSWs interfere and form dynamical density patterns (left panel in Fig. 1c) with a changing spatial periodicity. This temporal evolution presents an alternating sequence between quasi-periodic density peaks with large phase modulations (bottom) and less undulated density and phase profiles (top in the right panel). In our computations, each resulting peak near the center represents a phase-correlated Peregrine soliton-like structure [27]. We confirm the presence of a pair of near- π phase jumps across its core and tails; see Fig. 1c. Similar structures have been theoretically predicted in the integrable cubic focusing GPE model [29]. A Peregrine soliton was recently observed in a two-component repulsive gas [43].

In our experiment, initial density fluctuations also

seed MI, leading to the interplay between noise-amplified modulations and the DSWs. The former is randomly seeded in each realization, washing out the aforementioned localized structures in the sample-averaged density (Fig. 2a). The density profile near the boundaries, however, tends to shrink inwards shortly after the quench, indicating the emergence of the DSWs.

To analyze the quench dynamics reflecting both the DSWs and the noise-induced density modulations, we measure the density-density correlation function

$$C_n(\Delta x) = \frac{\langle n(x)n(x') \rangle}{\langle n(x) \rangle \langle n(x') \rangle} - 1, \quad (1)$$

where $\Delta x = |x - x'|$ and $\langle \dots \rangle$ denotes ensemble (around 20 samples) as well as spatial averaging. The correlation function estimates the second-order coherence, yielding density structure information—bunching ($C_n > 0$) or antibunching ($C_n < 0$) of densities separated by Δx . Figure 2b shows the observed dynamics of C_n within a spatial window of $|x|, |x'| \leq 15 \mu\text{m}$, representing density waves with dynamically changing periodicity for $t \lesssim 30$ ms. At early times $t \sim 7$ ms, density modulations with a short periodicity of $\sim 4 \mu\text{m}$ emerge, being clearly visible in the correlation profile depicted in Fig. 2c. This formation is attributed to fluctuation-seeded MI whose length scale $2\pi\xi \approx 4.4 \mu\text{m}$ is consistent with the observed periodicity, where $\xi = \hbar/\sqrt{2mn|g|}$ is the healing length [12, 17, 44]. At $t \sim 13$ ms roughly corresponding to the time scale of the DSW arrival at the box center [33], the noise-amplified modulation interacts with the DSWs. Their competition is evidenced through the transition in density modulations involving multiple spatial frequencies. At $t \gtrsim 31$ ms, a density modulation of $\sim 10 \mu\text{m}$

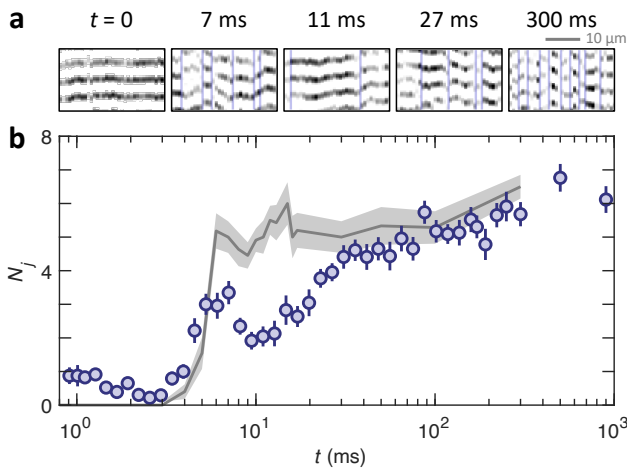


Fig. 3. **Observation of phase slips.** **a**, Interference fringes after the quench to the attractive scattering length $-5a_0$ discussed in Fig. 2. The vertical lines mark detected phase slips. **b**, Number of phase jumps N_j versus the hold time t after the interaction quench. Error bars indicate the standard error of the mean. Solid line shows the simulated N_j using the 2D GPE (≥ 6 samples for a given t). The shaded area represents the standard error of the mean.

periodicity prevails. We find that, at later times, the density-density correlation continues to evolve (see the last column in Fig. 2c).

To further visualize the many-body phase coherence characterizing the formation of density modulations, we evaluate the two-point phase correlation function

$$C_\phi(\Delta x) = \left\langle \text{Re} \left[e^{i\phi(x) - i\phi(x+\Delta x)} \right] \right\rangle, \quad (2)$$

which reveals the first-order coherence of the attractive Bose gas [33]. At $\Delta x > \xi$, non-zero $C_\phi(\Delta x)$ indicates finite-range phase correlations; $C_\phi \approx 0$ when the gas becomes phase uncorrelated or filled with random phase jumps. As shown in Fig. 2d, the measurement at $t = 0$ displays quasi-long-range coherence, decaying at a length $L \approx 16 \mu\text{m}$ that is consistent with interfering two prethermalized 1D gases after splitting from a condensate [3]; see also [33]. After the interaction quench $t > 0$, we observe remarkable dynamical coherence patterns. First, the gas retains finite-range phase correlations even after a periodic density modulation has emerged ($t \gtrsim 7$ ms). Second, when multiple spatial frequencies compete in the density modulation ($t \sim 13$ ms), we observe that the range of phase coherence transiently increases. At $t \gtrsim 31$ ms, the phase correlation gradually decreases to a shorter length scale. After sufficiently long hold times, the length scales of both density and phase correlations slowly approach the healing length ξ , as shown in Figs. 2e and f, respectively. We interpret this as the gas is filled with seemingly random density modulations and phase jumps, making the averaged correlation length shrink to $\sim \xi$.

Throughout the evolution, we expect phase jumps to accompany the formation of density modulations, as il-

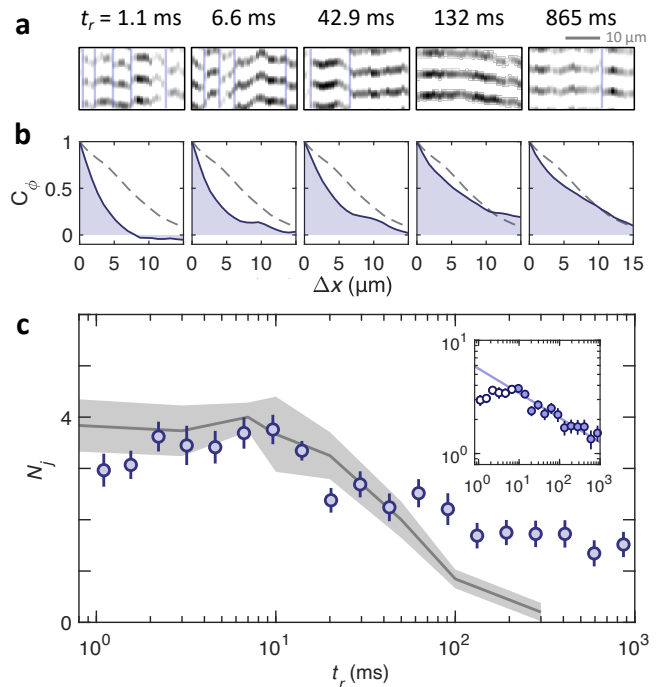


Fig. 4. **Observation of rephasing dynamics.** **a**, Interference fringes after holding the scattering length at $-5a_0$ for 50 ms followed by quench-up to the initial repulsion $105a_0$ within the ramp time t_r . The vertical lines mark the locations of the detected phase slips. **b**, The corresponding two-point phase correlation function C_ϕ . The dashed line in each panel represents the initial C_ϕ before quenching to attractive interactions. **c**, Number of phase jumps N_j as a function of t_r . Solid line represents N_j identified in 2D GPE simulations (≥ 8 samples at each t_r). The shaded area indicates the standard error of the mean. Inset shows the same data in the log-log scale along with a power-law fit (blue solid line) for data at $t_r > 10$ ms (filled circles).

lustrated in Fig. 1c. The evolution and loss of long-range phase coherence are traced back to the development of phase jumps. To visualize this connection, we count the number of fast phase slips, N_j , in the unwrapped $\phi(x)$ from the interference fringes (Fig. 3a); see also [33] for the details of phase slip counting. As shown in Fig. 3b, N_j grows with hold time, yet displaying a peak and a trough at $t \sim 7$ ms and ~ 11 ms, respectively, and afterwards demonstrating an increasing trend. This behavior is indeed responsible for the observed evolution of long-range phase coherence in Fig. 2d, complementing the dynamical structure formation observed in Fig. 2c.

In our experiments, finite transverse confinement along the y -axis, the initial noise, and the presence of atom loss alter the quench dynamics compared to a pure 1D case (Fig. 1c). To adequately model the emergent nonequilibrium behavior in our quasi-1D gases, we exploit a 2D GPE model considering these realistic conditions; see [33] for details. In our computations, we find prominent density undulations generated from the box edges and traveling towards the center in a sample averaged den-

sity, resembling the experimental images (Fig. 2a) and in line with the theoretical expectation from the corresponding dam-break system [29]; see Fig. S6 in [33] for comparison with Fig. 2. The simulated density-density and two-point phase correlation functions qualitatively reproduce the observed dynamical periodicity and finite-range phase coherence, with the exception that we have not observed the transient improvement of quasi-long-range phase coherence and a clear reduction of phase jumps around $10 \sim 13$ ms when the DSWs interact with the noise-induced density modulations; see Fig. 3b. At longer times, the time-averaged correlation lengths similarly drop to the healing length scale (see Fig. S6).

We now turn to the study of the rephasing dynamics starting from phase-scrambled attractive Bose gases. More specifically, after a sufficiently long hold time $t = 50$ ms when the phase correlation length shrinks to $\sim \xi$ (Fig. 2d), we ramp the interaction linearly back to its initial repulsive value within a variable time t_r (Fig. 1a). Figure 4a shows sample images of interference fringes taken at the end of the ramp. Under faster ramps, we observe that the fringes are more frequently interrupted by phase slips, suggesting the proliferation of density defects, that is, dark and gray solitons [45]. This can be understood as phase-incoherent domains start to merge at $g > 0$ and form density defects at the domain boundaries; see [33] and Fig. S7. Considerably larger phase-coherent domains are observed with slower ramps. For $t_r \gtrsim 132$ ms, the two-point phase correlations (Fig. 4b) show re-established quasi-long-range coherence. The length scale is remarkably comparable to that measured in the initial quasi-1D gas. This suggests that no significant heating was introduced during the attractive interaction stage, even after an attractive gas has seemingly lost its quasi-long-range phase coherence.

In Fig. 4c, we show the defect counting following the interaction ramp-back. With faster ramps, N_j roughly remains constant. For slow ramp-up times $t_r \gtrsim 10$ ms, the defect number gradually reduces, leading to improved phase coherence observed in Fig. 4b. With the longest $t_r \sim 1$ s, N_j reduces by around fourfold compared with the defect number before the ramp.

To qualitatively understand the observed rephasing behavior, we employ GPE simulations. We point out that, in an integrable 1D model, the phase slips generated in the attractive interaction regime convert to stable solitonic excitations regardless of the ramp-up time. Hence, N_j must be conserved. The 2D simulations, on the other hand, exhibit qualitatively similar rephasing dynamics as in the experiment after transitioning into the repulsive regime. The simulated number of phase jumps is de-

scribed in Fig. 4c, qualitatively reproducing the observed defect statistics except for long $t_r \gtrsim 100$ ms where we suspect that experimental imperfections such as finite heating could play a role to keep $N_j \gtrsim 1$.

It is crucial to emphasize the importance of the higher dimensionality in the rephasing dynamics, in line with observations such as those of [34]. As the interaction increases during the ramp-up, the healing length decreases to several times smaller than the transverse oscillator length l_y of the box trap. This allows solitonic excitations to convert into vortex dipoles [46–48], which can subsequently decay into sound waves via their collisions [49] and through drifting out from the gas [36], see also [33] for sample events observed in the 2D GPE simulations. We attribute the observed rephasing in Fig. 4 to these mechanisms. They result in a power-law decay in defect counting, as it was shown experimentally in a quasi-2D geometry [35]. Indeed, our data hint towards an approximate power-law scaling in the narrow 2D geometry with an extracted exponent ≈ 0.22 of detected phase jumps on ramp time t_r .

In conclusion, we report the observation of phase-coherent nonlinear dynamics in quasi-1D attractive Bose gases and their rephasing dynamics through interaction quenches between attraction and repulsion. Naturally, further systematic exploration of the role of dimensionality, by controllably modifying the geometry between quasi-1D and progressively more 2D settings, would be of considerable future interest in generating qualitatively different nonlinear dynamics [50] or in revealing possible connections between the observed rephasing and other spontaneous ordering mechanisms [36]. Additionally, as non-classical density correlations have been observed in attractive Bose gases [51], it would be intriguing to explore the role of beyond-mean field effects on the ensuing quench dynamics leveraging more sophisticated numerical methods [52].

ACKNOWLEDGMENTS

We thank Qi Zhou and Qiyu Liang for discussions. This work was supported in part by the NSF (Grant # PHY-2409591), the W. M. Keck Foundation, the DOE QuantISED program through the Fermilab Quantum Consortium, and the AFOSR (FA9550-22-1-0327). This material is also based upon work supported by the US National Science Foundation under Grant No. PHY-2110030, PHY-2408988 and DMS-2204702 (P.G.K.). S.I.M. acknowledges support from the Missouri University of Science and Technology, Department of Physics, Startup fund.

[1] M. H. Anderson, J. R. Ensher, M. R. Matthews, C. E. Wieman, and E. A. Cornell, Observation of Bose-Einstein

condensation in a dilute atomic vapor, *Science* **269**, 198 (1995).

- [2] C. Raman, M. Köhl, R. Onofrio, D. Durfee, C. Kulewicz, Z. Hadzibabic, and W. Ketterle, Evidence for a critical velocity in a Bose-Einstein condensed gas, *Phys. Rev. Lett.* **83**, 2502 (1999).
- [3] T. Langen, R. Geiger, M. Kuhnert, B. Rauer, and J. Schmiedmayer, Local emergence of thermal correlations in an isolated quantum many-body system, *Nature Phys.* **9**, 640 (2013).
- [4] B. Rauer, S. Erne, T. Schweigler, F. Cataldini, M. Tajik, and J. Schmiedmayer, Recurrences in an isolated quantum many-body system, *Science* **360**, 307 (2018).
- [5] P. Ilzhöfer, M. Sohmen, G. Durastante, C. Politi, A. Trautmann, G. Natale, G. Morpurgo, T. Giamarchi, L. Chomaz, M. Mark, *et al.*, Phase coherence in out-of-equilibrium supersolid states of ultracold dipolar atoms, *Nature Phys.* **17**, 356 (2021).
- [6] M. Prüfer, P. Kunkel, H. Strobel, S. Lannig, D. Linemann, C.-M. Schmied, J. Berges, T. Gasenzer, and M. K. Oberthaler, Observation of universal dynamics in a spinor Bose gas far from equilibrium, *Nature* **563**, 217 (2018).
- [7] C.-M. Schmied, M. Prüfer, M. K. Oberthaler, and T. Gasenzer, Bidirectional universal dynamics in a spinor Bose gas close to a nonthermal fixed point, *Phys. Rev. A* **99**, 033611 (2019).
- [8] S. Huh, K. Mukherjee, K. Kwon, J. Seo, J. Hur, S. I. Mistakidis, H. R. Sadeghpour, and J.-y. Choi, Universality class of a spinor Bose-Einstein condensate far from equilibrium, *Nature Phys.* **20**, 402 (2024).
- [9] S. Sunami, V. P. Singh, D. Garrick, A. Beregi, A. J. Barker, K. Luksch, E. Bentine, L. Mathey, and C. J. Foot, Universal scaling of the dynamic BKT transition in quenched 2d Bose gases, *Science* **382**, 443 (2023).
- [10] K. E. Strecker, G. B. Partridge, A. G. Truscott, and R. G. Hulet, Formation and Propagation of Matter-Wave Soliton Trains, *Nature* **417**, 150 (2002).
- [11] K. E. Strecker, G. B. Partridge, A. G. Truscott, and R. G. Hulet, Bright Matter Wave Solitons in Bose-Einstein Condensates, *New J. Phys.* **5**, 73 (2003).
- [12] J. H. Nguyen, D. Luo, and R. G. Hulet, Formation of matter-wave soliton trains by modulational instability, *Science* **356**, 422 (2017).
- [13] P. J. Everitt, M. A. Sooriyabandara, M. Guasoni, P. B. Wigley, C. H. Wei, G. D. McDonald, K. S. Hardman, P. Manju, J. D. Close, C. C. N. Kuhn, S. S. Szigeti, Y. S. Kivshar, and N. P. Robins, Observation of a modulational instability in Bose-Einstein condensates, *Phys. Rev. A* **96**, 041601 (2017).
- [14] J. M. Gerton, D. Strekalov, I. Prodan, and R. G. Hulet, Direct observation of growth and collapse of a Bose-Einstein condensate with attractive interactions, *Nature* **408**, 692 (2000).
- [15] E. A. Donley, N. R. Claussen, S. L. Cornish, J. L. Roberts, E. A. Cornell, and C. E. Wieman, Dynamics of collapsing and exploding Bose-Einstein condensates, *Nature* **412**, 295 (2001).
- [16] C. Eigen, A. L. Gaunt, A. Suleymanzade, N. Navon, Z. Hadzibabic, and R. P. Smith, Observation of weak collapse in a Bose-Einstein condensate, *Phys. Rev. X* **6**, 041058 (2016).
- [17] C.-A. Chen and C.-L. Hung, Observation of Universal Quench Dynamics and Townes Soliton Formation from Modulational Instability in Two-Dimensional Bose Gases, *Phys. Rev. Lett.* **125**, 250401 (2020).
- [18] S. L. Cornish, S. T. Thompson, and C. E. Wieman, Formation of Bright Matter-Wave Solitons during the Collapse of Attractive Bose-Einstein Condensates, *Phys. Rev. Lett.* **96**, 170401 (2006).
- [19] P. Medley, M. A. Minar, N. C. Cizek, D. Berryrieser, and M. A. Kasevich, Evaporative Production of Bright Atomic Solitons, *Phys. Rev. Lett.* **112**, 060401 (2014).
- [20] A. L. Marchant, T. P. Billam, T. P. Wiles, M. M. H. Yu, S. A. Gardiner, and S. L. Cornish, Controlled formation and reflection of a bright solitary matter-wave, *Nature Commun.* **4**, 1865 (2013).
- [21] G. D. McDonald, C. C. N. Kuhn, K. S. Hardman, S. Bennetts, P. J. Everitt, P. A. Altin, J. E. Debs, J. D. Close, and N. P. Robins, Bright Solitonic Matter-Wave Interferometer, *Phys. Rev. Lett.* **113**, 013002 (2014).
- [22] S. Lepoutre, L. Fouché, A. Boissé, G. Berthet, G. Salomon, A. Aspect, and T. Bourdel, Production of strongly bound ^{39}K bright solitons, *Phys. Rev. A* **94**, 053626 (2016).
- [23] V. E. Zakharov and A. A. Gelash, Nonlinear stage of modulation instability, *Phys. Rev. Lett.* **111**, 054101 (2013).
- [24] G. Biondini and D. Mantzavinos, Universal Nature of the Nonlinear Stage of Modulational Instability, *Phys. Rev. Lett.* **116**, 043902 (2016).
- [25] S. Mossman, S. I. Mistakidis, G. C. Katsimiga, A. Romero-Ros, G. Biondini, P. Schmelcher, P. Engels, and P. G. Kevrekidis, Nonlinear stage of modulational instability in repulsive two-component Bose-Einstein condensates, *arXiv:2412.17083* (2024).
- [26] N. N. Akhmediev and V. I. Korneeov, Modulation instability and periodic solutions of the nonlinear Schrödinger equation, *Theor. Math. Phys.* **69**, 1089 (1986).
- [27] D. H. Peregrine, Water waves, nonlinear Schrödinger equations and their solutions, *The ANZIAM Journal* **25**, 16 (1983).
- [28] N. Akhmediev, J. M. Soto-Crespo, and A. Ankiewicz, Extreme waves that appear from nowhere: on the nature of rogue waves, *Phys. Lett. A* **373**, 2137 (2009).
- [29] G. A. El, E. G. Khamis, and A. Tovbis, Dam break problem for the focusing nonlinear Schrödinger equation and the generation of rogue waves, *Nonlinearity* **29**, 2798 (2016).
- [30] J. M. Soto-Crespo, N. Devine, and N. Akhmediev, Integrable turbulence and rogue waves: breathers or solitons?, *Phys. Rev. Lett.* **116**, 103901 (2016).
- [31] N. Akhmediev, J. Soto-Crespo, and N. Devine, Breather turbulence versus soliton turbulence: Rogue waves, probability density functions, and spectral features, *Phys. Rev. E* **94**, 022212 (2016).
- [32] C. Mahnke and F. Mitschke, Possibility of an Akhmediev breather decaying into solitons, *Phys. Rev. A* **85**, 033808 (2012).
- [33] See Supplementary Material for more experimental and theory details.
- [34] C. Becker, K. Sengstock, P. Schmelcher, P. G. Kevrekidis, and R. Carretero-González, Inelastic collisions of solitary waves in anisotropic Bose-Einstein condensates: slingshot events and expanding collision bubbles, *New J. Phys.* **15**, 113028 (2013).
- [35] W. J. Kwon, G. Moon, J.-y. Choi, S. W. Seo, and Y.-i. Shin, Relaxation of superfluid turbulence in highly oblate Bose-Einstein condensates, *Phys. Rev. A* **90**, 063627 (2014).

- [36] T. Kanai and W. Guo, True mechanism of spontaneous order from turbulence in two-dimensional superfluid manifolds, *Phys. Rev. Lett.* **127**, 095301 (2021).
- [37] C. Chin, R. Grimm, P. Julienne, and E. Tiesinga, Feshbach resonances in ultracold gases, *Rev. Mod. Phys.* **82**, 1225 (2010).
- [38] T. Langen, S. Erne, R. Geiger, B. Rauer, T. Schweigler, M. Kuhnert, W. Rohringer, I. E. Mazets, T. Gasenzer, and J. Schmiedmayer, Experimental observation of a generalized Gibbs ensemble, *Science* **348**, 207 (2015).
- [39] T. Schweigler, V. Kasper, S. Erne, I. Mazets, B. Rauer, F. Cataldini, T. Langen, T. Gasenzer, J. Berges, and J. Schmiedmayer, Experimental characterization of a quantum many-body system via higher-order correlations, *Nature* **545**, 323 (2017).
- [40] S. Sharan, J. G. Sorribes, P. Sprenger, M. A. Hofer, P. Engels, B. Ilan, and M. Mossman, Breaking a superfluid harmonic dam: Observation and theory of rarefaction flow, riemann invariants and sonic horizon dynamics, arXiv preprint arXiv:2503.23246 (2025).
- [41] G. El and M. Hofer, Dispersive shock waves and modulation theory, *Phys. D* **333**, 11 (2016).
- [42] G. Biondini, Riemann problems and dispersive shocks in self-focusing media, *Phys. Rev. E* **98**, 052220 (2018).
- [43] A. Romero-Ros, G. C. Katsimiga, S. I. Mistakidis, S. Mossman, G. Biondini, P. Schmelcher, P. Engels, and P. G. Kevrekidis, Experimental realization of the peregrine soliton in repulsive two-component Bose-Einstein condensates, *Phys. Rev. Lett.* **132**, 033402 (2024).
- [44] L. Salasnich, A. Parola, and L. Reatto, Modulational instability and complex dynamics of confined matter-wave solitons, *Phys. Rev. Lett.* **91**, 080405 (2003).
- [45] D. J. Frantzeskakis, Dark solitons in atomic Bose-Einstein condensates: from theory to experiments, *J. Phys. A: Math and Theor.* **43**, 213001 (2010).
- [46] Y. S. Kivshar and D. E. Pelinovsky, Self-focusing and transverse instabilities of solitary waves, *Phys. Rep.* **331**, 117 (2000).
- [47] P. G. Kevrekidis, D. J. Frantzeskakis, and R. Carretero-González, *The Defocusing Nonlinear Schrödinger Equation: From Dark Soliton to Vortices and Vortex Rings*, Other Titles in Applied Mathematics (Society for Industrial and Applied Mathematics, Philadelphia, 2015).
- [48] H. Tamura, C.-A. Chen, and C.-L. Hung, Observation of self-patterned defect formation in atomic superfluids—from ring dark solitons to vortex dipole necklaces, *Phys. Rev. X* **13**, 031029 (2023).
- [49] W. J. Kwon, G. Del Pace, K. Khani, L. Galantucci, A. Muzi Falconi, M. Inguscio, F. Scazza, and G. Roati, Sound emission and annihilations in a programmable quantum vortex collider, *Nature* **600**, 64 (2021).
- [50] L. Dieli, D. Pierangeli, E. DelRe, and C. Conti, Observation of Two-Dimensional Dam Break Flow and a Gaseous Phase of Solitons in a Photon Fluid, *Phys. Rev. Lett.* **133**, 183801 (2024).
- [51] C.-A. Chen, S. Khlebnikov, and C.-L. Hung, Observation of quasiparticle pair production and quantum entanglement in atomic quantum gases quenched to an attractive interaction, *Phys. Rev. Lett.* **127**, 060404 (2021).
- [52] S. I. Mistakidis, A. G. Volosniev, R. E. Barfknecht, T. Fogarty, T. Busch, A. Foerster, P. Schmelcher, and N. T. Zinner, Few-body Bose gases in low dimensions—a laboratory for quantum dynamics, *Phys. Rep.* **1042**, 1 (2023).
- [53] M. Naraschewski and R. J. Glauber, Spatial coherence and density correlations of trapped Bose gases, *Phys. Rev. A* **59**, 4595 (1999).
- [54] M. Gring, M. Kuhnert, T. Langen, T. Kitagawa, B. Rauer, M. Schreitl, I. Mazets, D. A. Smith, E. Demler, and J. Schmiedmayer, Relaxation and prethermalization in an isolated quantum system, *Science* **337**, 1318 (2012).
- [55] R. Geiger, T. Langen, I. Mazets, and J. Schmiedmayer, Local relaxation and light-cone-like propagation of correlations in a trapped one-dimensional Bose gas, *New J. Phys.* **16**, 053034 (2014).
- [56] H.-P. Stimming, N. J. Mauser, J. Schmiedmayer, and I. E. Mazets, Dephasing in coherently split quasicondensates, *Phys. Rev. A* **83**, 023618 (2011).
- [57] G. A. El, E. G. Khamis, and A. Tovbis, Dam break problem for the focusing nonlinear Schrödinger equation and the generation of rogue waves, *Nonlinearity* **29**, 2798 (2016).
- [58] S. Banerjee, K. Zhou, S. K. Tiwari, H. Tamura, R. Li, P. Kevrekidis, S. I. Mistakidis, V. Walther, and C.-L. Hung, Collapse of a quantum vortex in an attractive two-dimensional Bose gas, arXiv preprint arXiv:2406.00863 (2024).

Supplementary Material for “Observation of many-body coherence in quasi-one-dimensional attractive Bose gases”

Hikaru Tamura,^{1,*} Sambit Banerjee,¹ Rongjie Li,¹ Panayotis Kevrekidis,^{2,3} Simeon I. Mistakidis,⁴ and Chen-Lung Hung^{1,5,†}

¹*Department of Physics and Astronomy, Purdue University, West Lafayette, IN 47907, USA*

²*Department of Mathematics and Statistics, University of Massachusetts Amherst, Amherst, Massachusetts 01003-9305, USA*

³*Department of Physics, University of Massachusetts Amherst, Amherst, Massachusetts 01003, USA*

⁴*Department of Physics and LAMOR, Missouri University of Science and Technology, Rolla, MO 65409, USA*

⁵*Purdue Quantum Science and Engineering Institute, Purdue University, West Lafayette, IN 47907, USA*

(Dated: June 17, 2025)

A. Preparation and detection of quasi-1D gases

We begin the experiment by loading a cesium Bose-Einstein condensate (BEC) into two quasi-1D box traps in 400 ms, followed by a 500 ms wait time to reach equilibrium. The initial scattering length is $105a_0$. The boxes are formed using 780 nm blue-detuned light [48]. The vertical box confinement is given by a single node of a $3\mu\text{m}$ -period optical lattice along the z -axis, while the horizontal confinement is produced by a rectangular repulsive potential barrier of $k_B \times 60\text{ nK}$ height, controlled by a digital mirror device (DMD). Here, k_B is the Boltzmann constant. The measured transverse trap frequencies are $\omega_z \approx 2\pi \times 2.2\text{ kHz}$ and $\omega_y \approx 2\pi \times 68\text{ Hz}$ along the z - and y -axes, respectively.

After initial preparation, we quench the scattering length to a negative value at $t = 0$ via a magnetic Feshbach resonance. After the interaction quench, we observe oscillations in the transverse width at a frequency of $\sim 2\omega_y$. The oscillation damps down quickly in 3 ms. After performing the experiments at various hold times t , we obtain in-situ or time-of-flight (TOF) density distribution in the horizontal (x - y) plane by absorption imaging with a resolution of $\approx 0.8\mu\text{m}$. In the rephasing experiments (Fig. 4), we perform the same imaging procedure after ramping up the attractive interaction back to the initial repulsive value and holding for 15 ms.

B. Relative phase measurement

To measure the spatially-resolved relative phase in two parallel quasi-1D gases, we shut off the potential in the x - y plane while keeping the vertical confinement, resulting in TOF expansion in the horizontal plane. The quasi-1D gases expand much more rapidly along the y direction, forming interference patterns. During the TOF, we quench the scattering length to nearly zero to avoid nonlinear fringe distortions [46].

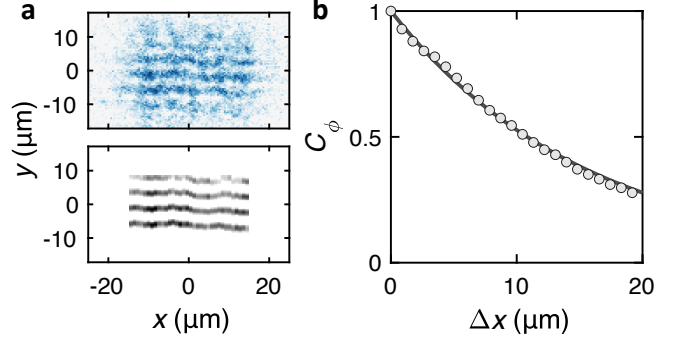


Fig. S1. **Experimental interference fringes and two-point relative phase correlation function.** **a**, A single-shot TOF density image (top panel), showing interference fringes of two expanding quasi-1D gases. The central region of the filtered TOF image (bottom panel) is analyzed to extract the relative phase $\phi(x)$ along the longitudinal direction. **b**, Initial two-point relative phase correlation function C_ϕ at repulsive scattering length $a \approx 105a_0$. Solid line is an exponential fit.

Figure S1a shows a sample density distribution imaged after 15 ms of TOF expansion. To clearly visualize the interference fringes, we apply a bandpass filter along the y -axis ($0.5\mu\text{m}^{-1} < k_y < 2\mu\text{m}^{-1}$ in the frequency domain). We extract the relative phase $\phi(x)$ from the central part of the fringe patterns ($|x| \leq 15\mu\text{m}$, $|y| \leq 8.6\mu\text{m}$) by fitting each density line-cut (along y -axis) with a sinusoidal function.

C. Two-point phase correlation function

We evaluate the relative phase correlation function of two interfering quasi-1D gases as

$$C_\phi(\Delta x) = \left\langle e^{i[\phi(x) - \phi(x')]} \right\rangle = e^{-\frac{1}{2}\langle \delta\phi^2 \rangle}, \quad (\text{S1})$$

where $\phi(x) = \varphi_1(x) - \varphi_2(x)$ is the local relative phase between two gases. Also, $\langle \delta\phi^2 \rangle = \left\langle [\phi(x) - \phi(x')]^2 \right\rangle$ is the two-point phase variance, $\Delta x = |x - x'|$ refers to the spatial separation, and $\langle \dots \rangle$ denotes ensemble and spatial

* tamurah@ims.ac.jp; Present address: Institute for Molecular Science, Okazaki, Aichi 444-8585, Japan

† clhung@purdue.edu

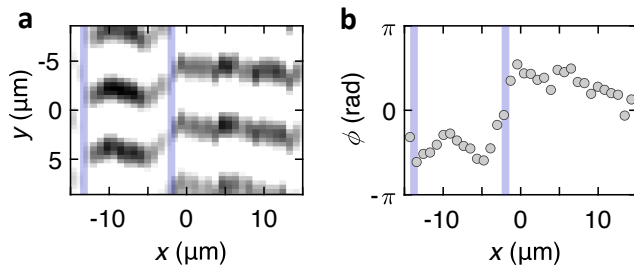


Fig. S2. **Experimental analysis of phase jumps.** **a**, Sample fringe pattern presenting phase jumps observed in the rephasing experiments. **b**, Corresponding relative phase $\phi(x)$. Vertical lines indicate the locations of detected phase jumps.

averaging. We have assumed that C_ϕ is an even function and hence only its real part is non-zero. For degenerate gases with homogeneous density profiles, this is equivalent to measuring the two-point correlation function

$$C_\phi(\Delta x) = \frac{\langle \psi_1(x)\psi_2^\dagger(x)\psi_1^\dagger(x')\psi_2(x') \rangle}{\langle |\psi_1(x)|^2 \rangle \langle |\psi_2(x')|^2 \rangle}, \quad (\text{S2})$$

where $\psi_j^{(\dagger)}$ is the bosonic field operator and $j \in 1, 2$ designates the gas in each quasi-1D box trap. One can obtain Eq. (S1) by substituting $\psi_j \approx \sqrt{n}e^{i\varphi_j(x)}$ into Eq. (S2) and using the 1D quasi-condensate density n (assumed to be the same in both boxes) and phase $\varphi_j(x)$. For two initial gases with independent phase fluctuations, one can further simplify the correlation function to

$$C_\phi(\Delta x) = |g^{(1)}(x, x')|^2, \quad (\text{S3})$$

where $g^{(1)}(x, x') = \langle \psi(x)\psi^\dagger(x') \rangle / n = \langle e^{i[\varphi(x) - \varphi(x')]} \rangle$ is the first-order coherence function. In this last expression, $C_\phi(\Delta x) \in [0, 1]$. When it is unity, the gas is fully coherent. Otherwise, coherence losses come into play evidencing the build-up of correlations in the system [53].

Initial correlation length

We measure $C_\phi(\Delta x)$ by spatially averaging $\text{Re}[e^{i\phi(x) - i\phi(x')}]$ over all points within the central region ($|x|, |x'| \leq 15 \mu\text{m}$). Figure S1b displays the recorded initial phase correlation function. We extract the correlation length $L = 15.6(2) \mu\text{m}$ using an exponential fit function $e^{-\Delta x/L}$. This corresponds to a coherence length of $L_c = 2L \approx 31 \mu\text{m}$ in the first-order coherence function.

Our sample preparation procedure appears to initiate parallel quasi-1D gases in a *prethermalized state*. For two segmented 1D gases emanating from a zero-temperature BEC, the projected phonons coherently evolve, yet appear dephased in the long-time limit, reaching a prethermalized state [54, 55]. The time-averaged variance of the relative phase is given by $\langle \delta\phi^2 \rangle = \frac{mg}{\hbar^2} \Delta x$. The effective

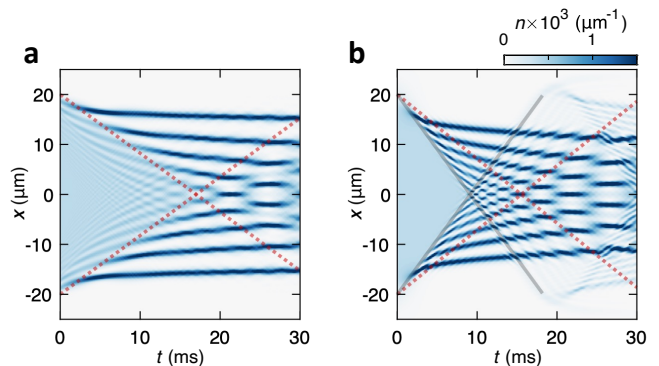


Fig. S3. **Numerical 1D simulations of shock wave generation and their interaction.** **a**, Density evolution under an infinite hard-wall potential following an interaction quench from $a = 105a_0$ to $-4.6a_0$. **b**, Same as **a**, but utilizing a Gaussian wall characterized by a width $w = 3 \mu\text{m}$. The red dotted lines show the theoretically predicted flow speed v assuming hard-wall confinement and initial density $400 \mu\text{m}^{-3}$. The gray solid lines in **b** provide a guide to the eye for monitoring the speed of flow emitted from the Gaussian wall.

coherence length $L_{\text{pre}} = 2\hbar^2/(mg) \approx 35 \mu\text{m}$ matches well to the measured $L_c \approx 31 \mu\text{m}$. On the other hand, if we consider initial phase fluctuations under thermal equilibrium [56], the expected coherence length in a quasi-condensate is $L_{\text{th}} = 2\hbar^2 n / (mk_B T)$. Comparing L_{th} with the measured L_c , the estimated initial temperature would reach $T \approx 94 \text{ nK}$, exceeding the energy barrier provided by the confining wall potential.

D. Phase slip detection

From the relative phases $\phi(x)$ obtained from the interference fringes (Fig. S2), we count the number of phase slips. We first unwrap $\phi(x)$ to remove 2π phase jumps and evaluate the phase gradient $\frac{d\phi}{dx}$. We then compare $\left| \frac{d\phi}{dx} \right|$ with an empirically selected lower bound threshold of $0.29\pi / \mu\text{m}$ to count phase slips. This is chosen to avoid falsely detecting smaller phase distortions as phase jumps. We have applied the same detection criteria to the entire data set presented in Figs. 3 and 4. The validity of the phase slip detection using 2D GPE simulations is also discussed below.

E. Dispersive shock waves in 1D GPE simulations

To understand various effects on the dynamics of dam-break flow in a simplified way, we perform time-dependent numerical simulations of the 1D Gross-Pitaevskii equation (GPE):

$$i\hbar \frac{\partial \psi}{\partial t} = \left[-\frac{\hbar^2}{2m} \frac{\partial^2}{\partial x^2} + g|\psi|^2 + V(x) \right] \psi, \quad (\text{S4})$$

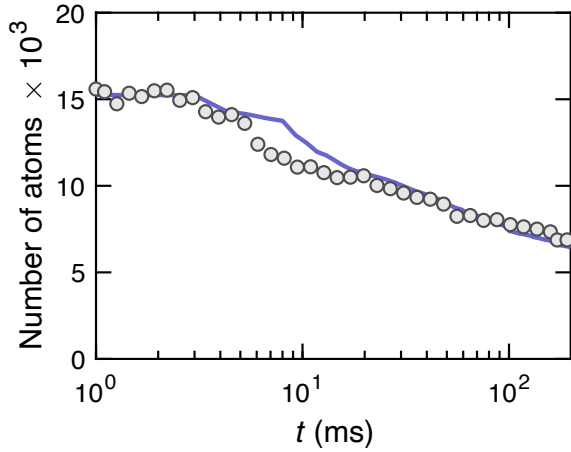


Fig. S4. **Observation of atom loss.** Measured atom number (circles) versus hold time t at the attractive scattering length $a \approx -5a_0$. The standard error is comparable to or smaller than the marker size. The solid line represents the sample-averaged atom number evaluated using the 2D GPE simulations.

where $\psi(x, t)$ represents the 1D mean-field wavefunction and $V(x)$ is the potential well.

Dynamics of quenched box-trapped gases is in accordance with the expectation from the underlying dam-break problem. In a situation where the confining potential has infinite hard walls and a length l (Fig. S3a), DSWs from the boundaries are expected to propagate at a dominant speed $v = \frac{2\hbar}{m\xi}$ (dotted line) [57], irrespective of the box length. This is indeed well captured by the simulated dynamics. Here, $\xi = \hbar/\sqrt{2mn_0|g|}$ is the healing length and n_0 is the initial homogeneous density. The counter-propagating flows weakly interfere with each other, and apparently different structures appear at around $t_c = l/(2v)$. We find that Peregrine soliton-like structures spontaneously form initially around $x = 0$, while the number of such structures dynamically increases, in line with the theoretical prediction of [29]. Those are represented by multiple near π -phase jumps across each density peak and its tails. The generated density peaks near $x = 0$ can be well approximated by the analytical Peregrine waveform.

In experiments, the sharpness of the box wall is softened due to finite optical resolution. This feature is well approximated by the potential

$$V(x) = \frac{U_0}{2} \left[1 + \operatorname{erf} \left(\frac{|x| - l/2}{w} \right) \right], \quad (\text{S5})$$

characterized by width w and dictated by the error function $\operatorname{erf}(x)$. The simulated 1D GPE dynamics reveals that the soft wall accelerates the evolution of the counterpropagating DSWs when we compare Fig. S3 a (hard-wall) and b (finite $w > 0$). However, similarly to the hard-wall potential, the emitted DSWs collide at the center and subsequently produce an array of Peregrine

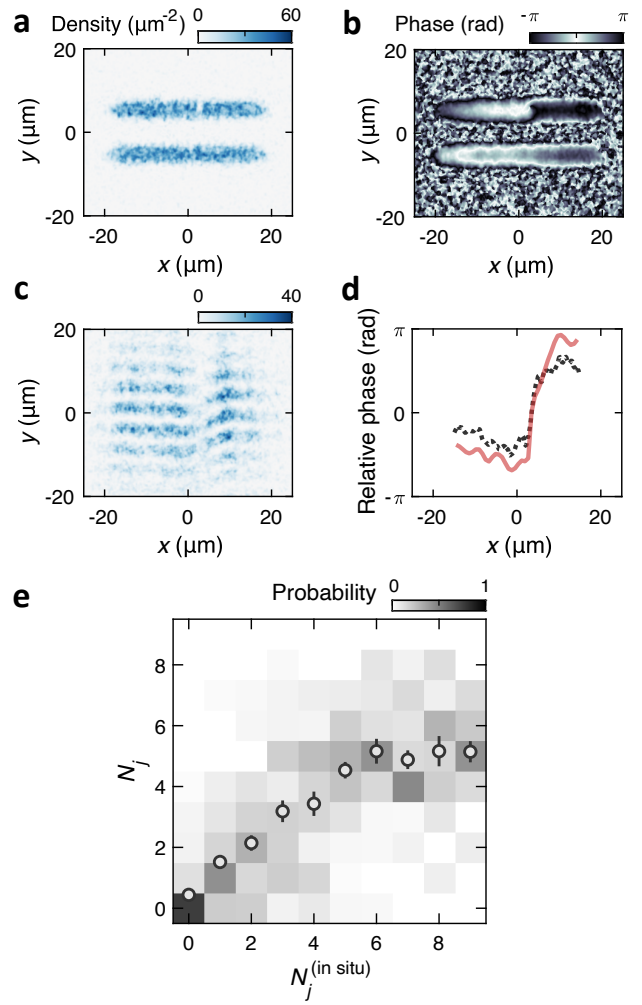


Fig. S5. **2D GPE simulations of matter-wave interference.** **a**, Simulated density profiles of two parallel quasi-1D samples at the end of the interaction ramp-up procedure as depicted in Fig. 1(a3). **b**, The corresponding phase profiles. **c**, Simulated density image after 15 ms of TOF expansion. **d**, Relative phase between the two clouds; $\phi(x)$ determined by the interference fringes (red solid line) and $\phi_1 - \phi_2$ obtained from the in-situ phase difference (black dotted line), respectively. **e**, Number of phase jumps, N_j , identified in the simulated TOF fringes (scatter plots) versus the number of jumps in the in-situ phase profile, $N_j^{(\text{in situ})}$. Error bars represent the standard error of the mean. Colormap represents probability of detecting N_j slips for a given $N_j^{(\text{in situ})}$. Counting statistics is obtained by analyzing ≈ 450 simulations samples in total following the same procedures as the experiments in Fig. 3 or Fig. 4 with different hold or ramp-up times ($t, t_r \leq 300$ ms).

soliton-like structures; see Fig. S3b.

F. 2D GPE simulations

The 1D simulations offer an idealized picture of the experimentally observed dynamics due to several rea-

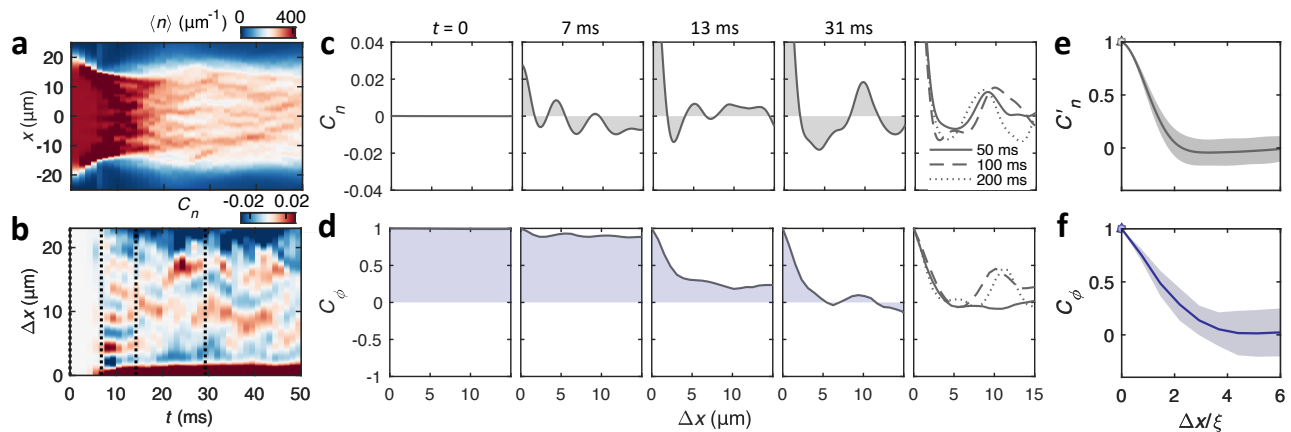


Fig. S6. **Dynamical density modulations and phase coherence in 2D GPE simulations.** **a**, Time evolution of the sample-averaged density profile after a quench of the s-wave scattering length from $a = 105a_0$ to $-4.6a_0$. The plotted 1D density along the x -axis results from integrating the 2D density over the transverse direction. **b**, Dynamics of density-density correlation function $C_n(\Delta x)$ with two-point separation Δx . **c**, $C_n(\Delta x)$ at the characteristic times marked by the dashed lines in **b** and at the indicated long hold times. **d**, Two-point phase correlation function $C_\phi(\Delta x)$, evaluated at the same times as **c**, from numerically simulated interference patterns of two independent samples. **e**, $C'_n = C_n(\Delta x)/C_n(0)$ and **f**, C_ϕ versus rescaled length $\Delta x/\xi$. Both C'_n and C_ϕ are time-averaged over samples after hold time $t = 50$ ms up to $t = 300$ ms. The shaded areas represent the standard deviation from the mean. The simulations follow the experimental procedures and parameters as those used in Fig. 2 and account for the finite resolution effect; see [33].

sons. Firstly, in our experimental platform, the confining potential does not completely suppress transverse excitations (along y -axis) following the interaction quench. Secondly, there is initial noise (with quantum and thermal origins) in the initial gas. Thirdly, three-body loss is inevitably present in ultracold gases, especially so with higher densities. For these reasons, next we perform 2D GPE computations taking into account the aforementioned contributions in order to more accurately simulate the experimental conditions. The 2D confining potential now reads $V_{2D}(x, y) = V(x)\exp\left(-\frac{2y^2}{w_y^2}\right)$, where w_y is the transverse box width and $V(x)$ is described by Eq. (S5). We have added an empirical three-body loss term $-i\frac{\hbar}{2}L_3^{(2D)}|\psi|^4\psi$ to the 2D GPE to phenomenologically capture the experimentally observed slow atom loss. The effective three-body loss coefficient is given by $L_3^{(2D)} = L_3/3! \times 1/(\sqrt{3}\pi l_z^2)$. We have adopted a small 3D recombination loss rate, $L_3 = 5.5 \times 10^{-30}$ cm⁶/s, to match the simulated atom number with the experimentally measured atom loss curve as presented in Fig. S4. Note that the adopted value of L_3 is significantly smaller than those observed in Refs. [17, 58], where the gases undergo wave collapse in quasi-2D and suffer significant atom loss.

To capture the experimental conditions, we also include initial density fluctuations in the pre-quench gases. For this, we empirically seed noise to the GPE predicted zero temperature ground-state density profile $n_0 = |\psi|^2$. This is achieved through $n = n_0(1 + \eta)$, where the noise term $\eta = \sum_k \frac{n_k}{N_a} \sin(kx + \delta_k)$. Here, N_a is the total particle number, k represents the momentum wavenumber, and δ_k is a random phase uniformly distributed within

$[-\pi, \pi]$. Furthermore, to involve phase noise we consider $\varphi = \sum_k \varphi_k \sin(kx + \delta_k)$. The amplitudes $n_k = \langle |n(k)| \rangle$ and $\varphi_k \approx \langle |\phi(k)| \rangle / 2$ are obtained from the Fourier spectrum of the experimentally measured in-situ density and relative phase profiles, respectively. These amplitudes are further rescaled to match the simulated quench dynamics with experiments. We then evolve the obtained 2D wavefunction $\psi = \sqrt{n}e^{i\varphi}$ for a few milliseconds. Subsequently, this wavefunction is employed as the initial condition for the quench dynamics. Figure S6 illustrates 2D GPE simulation results in comparison with Fig. 2 (see also the discussion in the main text). We note that the simulated dynamics shows overall qualitative agreement with the experiment (Fig. 2). However, to match the time scale for developing the characteristic features observed in the density-density correlations, we adopt samples with smaller noise, which results in also better coherence after a long hold time $t \geq 100$ ms. Here, the density-density correlations at $\Delta x \sim 10 \mu\text{m}$ remain partially phase coherent (the last columns in **c** and **d**). The dynamics of phase-slip counts (solid lines in Fig. 3b and Fig. 4c) are simulated with the same noise amplitude as measured in the experiment, and qualitatively capture the observation, see also Sec. G.

G. Validity of phase slips detection

To fully emulate the relative phase measurements discussed in the main text, we evolve two isolated wavefunctions and interfere them via TOF in the 2D GPE calculations. Figures S5a and b depict samples of simulated in-situ density and phase profiles emulating the experi-

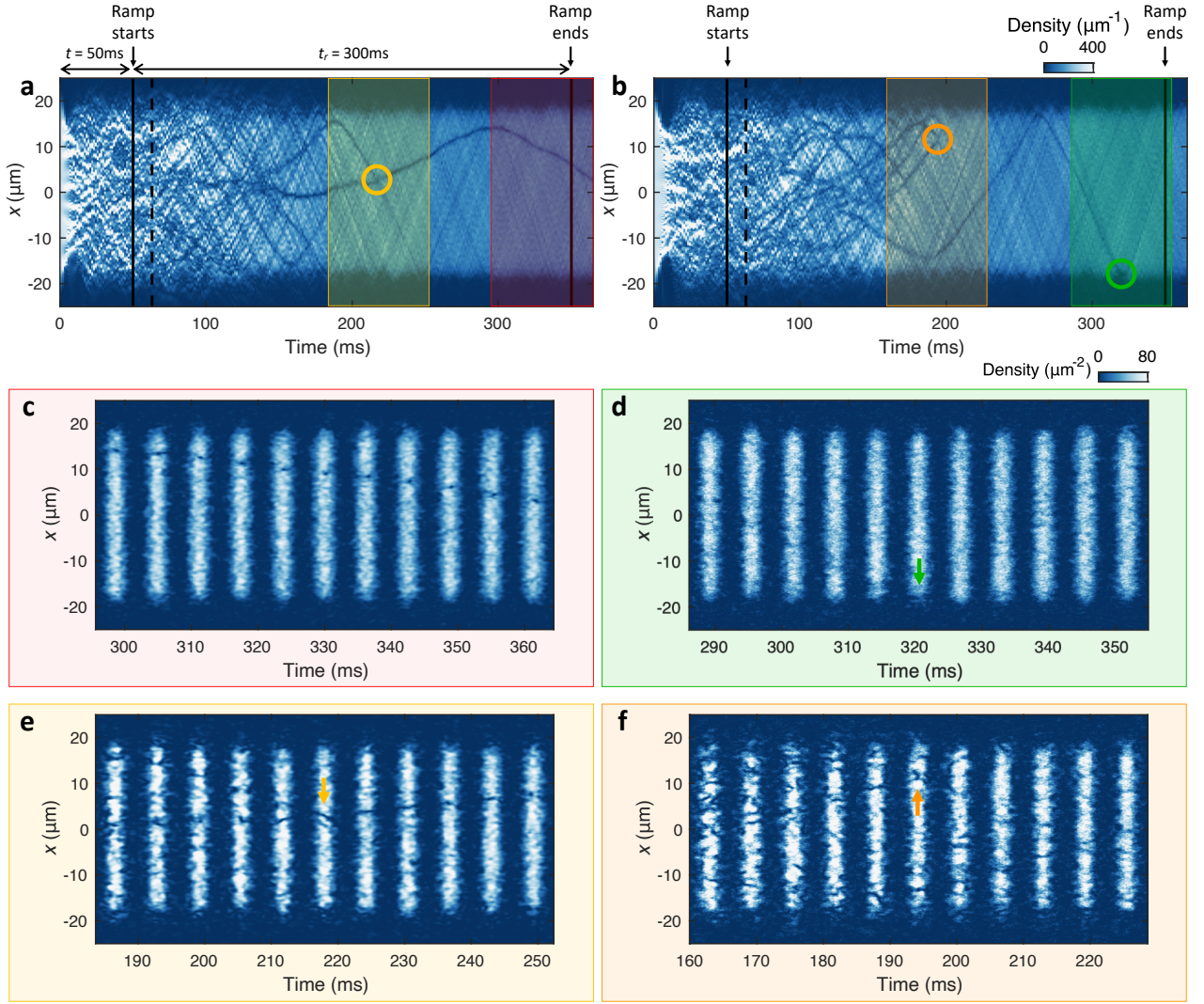


Fig. S7. **Defect annihilation and propagation dynamics identified in a quasi-1D gas in 2D GPE simulations.** **a** and **b**, Simulated time evolution of density profiles after an interaction quench-down from $a = 105a_0$ to $-4.6a_0$ and with different initial random noise. During the time evolution, the scattering length is kept constant for a hold time $t = 50$ ms and then is ramped back to the initial value in $t_r = 300$ ms, as indicated. Dashed line represents a time at which the scattering length crosses the zero value. The 2D density profiles are integrated over the transverse (y -)axis and the resulting 1D profiles are displayed along the x -axis. Color shaded areas in **a** (**b**) highlight events of sample defect dynamics, where the 2D densities within the corresponding time periods are plotted in **c** (red) and **e** (yellow) [**d** (green) and **f** (orange)], respectively. **c-f**, Time evolution of 2D density showing highlighted events: propagation of a vortex dipole-like defect (**c**), collision of a vortex dipole-like defect with the boundary (**d**), and inelastic defect collision events (**e** and **f**). Arrows indicate the locations of collision events, same as the circles in **a** and **b**.

mental procedure presented in Fig. 1(a3). Following the TOF expansion, we convolve the simulated density profiles with finite image resolution; see Fig. S5c. We then analyze the relative phase ϕ from the interference patterns as described in Sec. B. Figure S5d shows that the results are in qualitative agreement with the phase difference $\varphi_1 - \varphi_2$ directly extracted from the in-situ phase profile weighted-averaged using the mean density. We note that, as the TOF time increases, small-scale fluctuations can be washed out. Therefore, we limit the expansion time to 15 ms in our experiments. To confirm the validity

of phase slip detection, we compare the number of phase slips in TOF fringes, N_j , with the one directly obtained from $\varphi_1 - \varphi_2$, denoted as $N_j^{(\text{in situ})}$. Figure S5e shows the detected N_j averaged over samples having $N_j^{(\text{in situ})}$ slips. This comparison indicates nearly one-to-one correspondence between in situ and interference measurements for smaller $N_j^{(\text{in situ})}$. This justifies the validity of our observations at $t \lesssim 40$ ms in Fig. 3b and $t_r \gtrsim 10$ ms in Fig. 4c. When the density of phase slips increases, each phase slip appears to be less visible, leading to the under-counting,

see Fig. S5e.

H. Rephasing Dynamics

We study the rephasing dynamics by employing 2D GPE simulations closely following the experimental procedure. Prototypical examples of the simulated dynamics are shown in Fig. S7. In the early times of the ramp, it can be readily seen that the intense density modulation, developed during the epoch of attractive interactions, gradually smoothens out. The coherent domains appear to merge and spontaneously form density defects at the domain boundaries.

At later times of the ramp, as the interaction approaches the final value, these defects noticeably transition into vortex dipoles-like profiles due to the extended dimensionality ($\xi < l_y$). For instance, in Fig. S7a, one can see the propagation of a dark stripe at times $\gtrsim 220$ ms propagating with almost un-altered darkness (density contrast). The corresponding 2D images (Fig. S7c) show two weakly isolated cores, featuring a

vortex dipole-like profile.

These vortical defects are subject to inelastic collisions and annihilation; see, e.g., [34] for a relevant discussion. During the ramp, when enough defects form, we find intricate collisions between the density defects. At time ~ 218 ms in Fig. S7a, two dipole-like defects collide with one becoming indiscernible afterwards; see the 2D images in Fig. S7e. It is worthwhile to note that in the setting of the latter panel, the structure appears to clearly acquire the form of a single vortex (rather than a vortex dipole) in the confined geometry. Another collision event can be found at ~ 194 ms in Figs. S7b and f, showcasing similar dynamical features upon long-time evolution.

The defects can also interact with the boundary and disappear. In Fig. S7b, a propagating dipole collides with the box boundary at ~ 320 ms. This dramatically reduces its darkness (contrast), associated with vortex annihilation. The dipole becomes indiscernible after the collision in the corresponding 2D images (Fig. S7d).

Through collisions or interactions with the boundary, the density defects decay into sound, resulting in reduced phase jumps and improved phase coherence. We attribute the observed rephasing to these mechanisms.